Further Enhancement of the Thermostability of *Hydrogenobacter thermophilus* Cytochrome c_{552}[†]

Yo-ta Takahashi,[‡] Hiroaki Sasaki,[‡] Shin-ichi J. Takayama,[‡] Shin-ichi Mikami,[‡] Shin Kawano,[‡] Hajime Mita,[‡] Yoshihiro Sambongi,[§] and Yasuhiko Yamamoto*[,‡]

Department of Chemistry, University of Tsukuba, Tsukuba 305-8571, Japan, and Graduate School of Biosphere Science, Hiroshima University, Higashi-Hiroshima 739-8528, Japan

Received June 12, 2006; Revised Manuscript Received July 21, 2006

ABSTRACT: Thermophile *Hydrogenobacter thermophilus* cytochrome c_{552} (HT) is a stable protein with denaturation temperatures (T_m) of 109.8 and 129.7 °C for the oxidized and reduced forms, respectively [Uchiyama, S., Ohshima, A., Nakamura, S., Hasegawa, J., Terui, N., Takayama, S. J., Yamamoto, Y., Sambongi, Y., and Kobayashi, Y. (2004) *J. Am. Chem. Soc. 126,* 14684−14685]. The removal of a single hydroxyl group from the hydrophobic core of HT, through the replacement of a Tyr by Phe, resulted in further elevation of the T_m value of the oxidized form by ∼6 °C, the T_m value of the reduced one remaining essentially unaltered. As a result, the redox potential of the mutant with higher stability in the oxidized form exhibited a negative shift of ∼20 mV relative to that of wild-type HT in an enthalpic manner. These findings indicated that the redox function of a protein can be enthalpically regulated through the stability of the oxidized form by altering the contextual stereochemical packing of hydrophobic residues in the protein interior using protein engineering.

There is enormous interest in delineating the structural determinants underlying the thermostability of proteins. Apart from allowing a deeper understanding of protein architecture and evolution, this knowledge holds great promise for designing proteins for industrial use. Proteins isolated from thermophilic organisms have been extensively investigated from both experimental and theoretical points of view in order to gain such knowledge (*1*). In particular, comparative studies of the structures of homologous proteins of thermophiles and mesophiles have contributed significantly to the understanding of the relationship between protein structure and thermostability (*1*−*12*).

Thermophile *Hydrogenobacter thermophilus* cytochrome c_{552} (HT)[1] and mesophile *Pseudomonas aeruginosa* cytochrome c_{551} (PA) are small monoheme-containing electron transfer proteins composed of 80 and 82 amino acid residues, respectively. The two proteins exhibit high sequence identity (56%) (*13*), and their main-chain folding is almost identical (*2*). Despite their structural similarity, there is remarkable disparity in their thermostability and redox properties; the denaturation temperatures (T_m) of PA in both the reduced and oxidized forms are considerably lower than those of HT in the corresponding forms, and the redox potential (E_m) of PA at pH 6.0 and 25 °C is higher by ∼60 mV relative to that of HT (*5*, *6*, *8*) (Table 1). A detailed comparison of the protein interior between HT and PA revealed sizable differences in the packing of amino acid side chains, and site-directed mutants of PA, for which amino acid substitutions were selected with reference to the corresponding residues in HT, exhibited thermostabilities between those of the two proteins (*3*−*5*). These studies unequivocally demonstrated that the contextual stereochemical packing of hydrophobic residues is crucial for increased hydrophobic interaction conferring overall thermostability to proteins.

In the case of cyt *c*, in which the redox-dependent structure change is almost negligible (*14*, *15*), the protein stability has a paramount effect on its redox activity. The Gibbs energy change for the reduction of the oxidized protein, ΔG_{redox}, is expressed by the equation (*16*, *17*):

$$\Delta G_{redox} = \Delta G_{RC} + \Delta G_{EI}$$

where ΔG_{RC} is the Gibbs energy difference between the oxidized and reduced forms resulting from bonding interactions at the redox center and ΔG_{EI} accounts for the Gibbs energy difference in electrostatic stabilization between ferriheme in the oxidized form and ferroheme in the reduced one. The enhancement of protein stability through reinforcement of the hydrophobic core by mutations is expected to alter the ΔG_{RC} value, because the stability of an oxidized protein has been shown to be more greatly affected by

[†] This work was supported by a research grant (no. 17350081) from the Ministry of Education, Science, Sports, Culture, and Technology, the Yazaki Memorial Foundation for Science and Technology, the NOVARTIS Foundation (Japan) for the Promotion of Science, and the University of Tsukuba, Research Project (A).

* Corresponding author. Phone/Fax: +81-29-853-6521. E-mail: yamamoto@chem.tsukuba.ac.jp.

[‡] University of Tsukuba.

[§] Hiroshima University.

[1] Abbreviations: E_m, redox potential; cyt *c*, cytochrome *c*; PA, *Pseudomonas aeruginosa* cytochrome c_{551}; HT, *Hydrogenobacter thermophilus* cytochrome c_{552}; T_m, denaturation temperature of protein; $T_{m(Fe-Met)}$, dissociation temperature of Fe−Met bond; T_c, transition temperature; CV, cyclic voltammetry; E_m−pH plots, plots of redox potentials of proteins against pH; E_m−*T* plots, plots of redox potentials of proteins against temperature.

10.1021/bi061164g CCC: $33.50
Published on Web 08/19/2006

Table 1: Thermodynamic Parameters of the Redox Reaction for Wild-Type HT and PA and Their Y27F Mutants

	T_m[a] (°C)				ΔH[d] (kJ mol^{-1})		ΔS[d] (J K^{-1} mol^{-1})	
	oxidized	reduced	$T_{m(Fe-Met)}$[b] (°C)	ΔE_m[c] (mV)	low	high	low	high
HT	109.8[e]	129.7[e]	>100	243	−32.2	−37.5	−28.4	−45.7
HT(Y27F)	116	130	>100	224	−31.2	−36.5	−28.5	−44.7
PA	82.1[e]	109.0[e]	79	303	−47.0		−64.5	
PA(Y27F)	91	109	90	264	−44.1		−63.2	

[a] The unfolding temperatures (T_m) of the proteins were determined through analysis of the temperature dependence of the CD ellipticity at 222 nm. The experimental errors for the oxidized and reduced proteins were ±1.0 and ±2.0 °C, respectively. [b] The dissociation of the Fe−Met coordination bond of the oxidized protein at pH 7.0, determined from the temperature dependence of the 695 nm absorption band characteristic of the bond. The experimental errors were ±0.5 °C. [c] The redox potential is given in mV, with reference to a standard hydrogen electrode at 25 °C, pH 6.0. The experimental errors were ±5 mV. [d] The experimental errors for enthalpy (ΔH) and entropy (ΔS) were ±3 kJ mol^{-1} and ±10 J K^{-1} mol^{-1}, respectively. [d] Obtained from ref *9*.

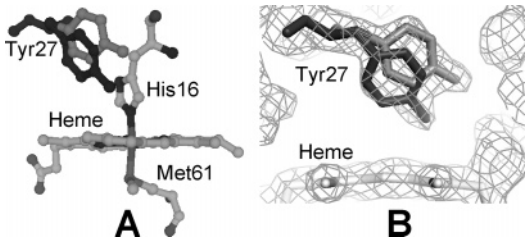

FIGURE 1: Schematic representation of Tyr17, together with heme, His16, and Met61, in *Hydrogenobacter thermophilus* cytochrome c_{552} (HT) (A) and the conformation of the Tyr27 side chain in the oxidized HT (PDB code 1YNR) (*18*) (B). The $2F_o - F_c$ map around the Tyr27 residue in HT is contoured at the 0.8 level. The electron density map was calculated with program PREMAC5 (*38*). These representations were drawn with PyMOL (*39*).

mutations than that of the reduced one (*9*). As a result, the E_m value of a mutant with higher stability is expected to exhibit a negative shift relative to that of the wild-type protein (*8*, *10*). Furthermore, we have also demonstrated in studies on PA and HT as well as a series of PA mutants that the overall protein stability correlates with the Fe−Met bond stability. Consequently, the E_m value of a protein is related to the Fe−Met bond stability (*7*, *8*, *10*).

According to the X-ray structure of HT (*18*), the side chain of Tyr27 (the numbering system for amino acids of HT corresponds to that for PA) is buried in the hydrophobic protein interior near the heme, its OH group being hydrogen-bonded to the sulfur atom of Met13. The Tyr27−Met13 hydrogen bonding is not sufficiently stable to force a single orientation of the Tyr27 side chain (Figure 1) and possibly makes an unfavorable contribution to the stability of the protein interior. Tyr27 is conserved in PA, but its side chain does not participate in a hydrogen bond because Val occupies position 13 (*19*). Hence, the OH group of the Tyr27 side chain in PA is also unfavorable for the stability of the hydrophobic core of the protein. Consequently, the replacement of Tyr27 by Phe in HT as well as PA is expected to reinforce the hydrophobic core of the protein, leading to enhancement of the protein stability.

In the present study, we extended our efforts to further stabilize the hydrophobic core of HT and PA through the removal of a hydroxyl group, i.e., replacement of Tyr27 by Phe, from the hydrophobic core in order to create proteins even more thermostable than the wild-type proteins and to gain a deeper understanding of the role of the hydrophobic core in the E_m regulation of the protein. In order to achieve these goals, single mutants, Y27F, of HT and PA (HT(Y27F) and PA(Y27F), respectively) were prepared and subjected to a detailed study on the structure−function relationship using paramagnetic NMR, circular dichroism (CD) measurements in the temperature range of 30−165 °C, absorption spectroscopy, and cyclic voltammetry (CV). The study demonstrated that the stability of the oxidized proteins was greatly increased by mutations, whereas that of the reduced ones was essentially unaltered. The different effects of the mutations on the stability of the two different redox forms of the protein resulted in a negative shift in the E_m value through the ΔG_{RC} contribution. The study demonstrated that the structural properties of the hydrophobic core in the protein interior are crucial for control of the redox function of the proteins.

MATERIALS AND METHODS

Protein Samples. The wild-type HT and PA and their mutants were produced using *Escherichia coli* and purified as reported previously (*3*, *4*). The oxidized forms of the proteins were prepared by the addition of a 10-fold molar excess of potassium ferricyanide. For NMR samples, the proteins were concentrated to about 1 mM in an ultrafiltration cell (YM-5, Amicon), and then 10% ^2H_2O was added to the protein solutions. The pH of each sample was adjusted using 0.2 M KOH or 0.2 M HCl, and the pH was monitored with a Horiba F-22 pH meter with a Horiba type 6069-10C electrode.

Cyclic Voltammetry. The procedures used for obtaining cyclic voltammograms for the proteins were essentially the same as those described previously (*8*, *20*−*22*). CV experiments were performed with a potentiostat-galvanostat PG-STAT12 (Autolab). A gold electrode treated with 4,4′-dipyridyl disulfide just before use was employed as the working electrode. An Ag|AgCl electrode in a saturated NaCl solution and a Pt wire were employed as the reference and counter electrodes, respectively. The potential sweep range was +350 to −150 mV vs the Ag|AgCl electrode in a saturated NaCl solution with a scan rate of 20 mV s^{-1}. All potentials are referenced to the standard hydrogen electrode. The protein concentration was about 0.5 mM in 20 mM phosphate buffer, pH 4.0−9.0, and 0.1 M $NaClO_4$. All experiments were performed at 25 °C under a nitrogen atmosphere. The anodic to cathodic peak current ratios obtained at various potential scan rates (1−100 mV s^{-1}) were all ∼1. Both the anodic and cathodic peak currents increased linearly as a function of the square root of the scan rate in the range up to 100 mV s^{-1}. The anodic and cathodic peak separations of the scan rate in the range up to 100 mV s^{-1} were approximately 100 mV. Thus, HT and

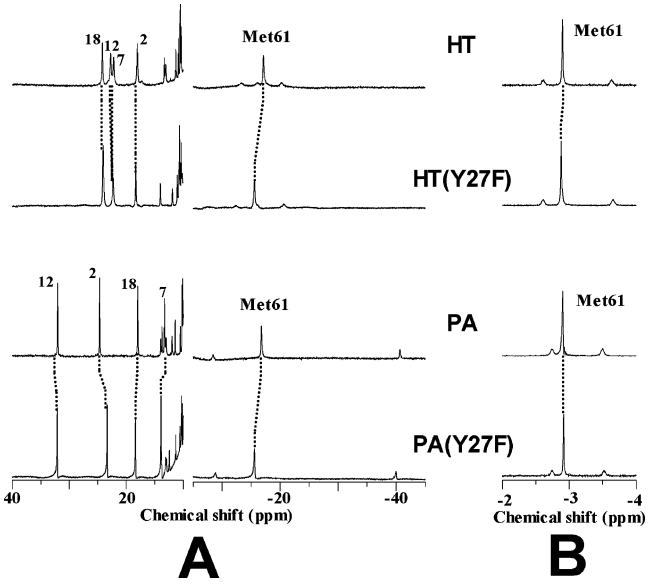

FIGURE 2: The downfield- and upfield-shifted portions of the 600 MHz ^{1}H NMR spectra of the oxidized forms of HT, HT(Y27F), PA, and PA(Y27F) in 90% H_2O/10% D_2O, pH 7.20, at 25 °C (A) and the upfield-shifted portions of the spectra of the reduced proteins under identical solution conditions (B). The corresponding heme methyl and Fe-coordinated Met61 methyl proton signals are connected by a broken line, with the signal assignments. The spectral patterns of the mutants are almost identical to those of the corresponding wild-type proteins, suggesting that the protein structures were essentially unaffected by the mutations.

PA and their mutants exhibit quasi-reversible redox processes.

^{1}H NMR. NMR spectra were recorded on a Bruker Avance 600 FT NMR spectrometer operating at the ^{1}H frequency of 600 MHz. Chemical shifts are given in ppm downfield from sodium 2,2-dimethyl-2-silapentane-5-sulfonate with H_2O as an internal reference.

Circular Dichroism Spectroscopy. CD spectra were recorded on a JASCO J-820 spectrometer over the spectral range of 20−300 nm and in the temperature range of 30−165 °C, using an airtight pressure-proof cell compartment with quartz windows, which was described previously (*9*).

Absorption Spectroscopy. Absorption spectra at 695 nm were recorded with a Beckman DU 640 spectrophotometer using a micro T_m analysis system and a micro T_m cell. The protein concentration was about 0.2 mM in 20 mM phosphate buffer, pH 7.0, in the presence of 10 mM potassium ferricyanide.

RESULTS

^{1}H NMR Spectra of the Mutants. We first analyzed the effects of the mutations on the heme active site of the proteins by means of paramagnetic ^{1}H NMR (Figure 2A). Paramagnetically shifted signals arising from heme peripheral methyl and Fe-coordinated Met61 protons were resolved in downfield- and upfield-shifted regions of the spectra, respectively. These signals have been shown to be extremely sensitive to the heme environment (*23*−*25*). In particular, the coordination structures of both axial His16 and Met61 contribute significantly to the paramagnetic shifts of the individual heme methyl proton signals of the oxidized proteins. In the present proteins, the conformation freedom of the axial His16 side chain is considerably restricted due to the covalent attachment

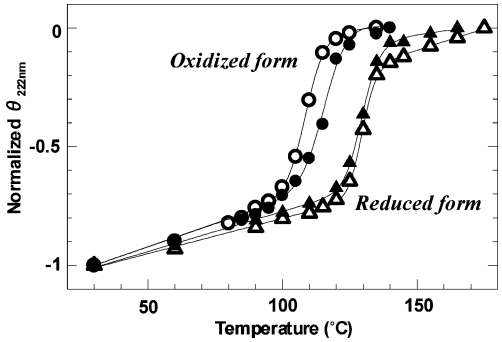

FIGURE 3: Unfolding profiles of HT in the oxidized (open circles) and reduced (open triangles) forms and HT(Y27F) in the oxidized (filled circles) and reduced (filled triangles) forms at pH 7.0.

of heme to the protein moiety, with the coordination of the His imidazole to heme iron, through the heme attachment motif Cys-x-z-Cys-His (x and z represent arbitrary amino acid residues) and the hydrogen bonding of the His $N_\delta H$ proton with surrounding residues (*18*, *19*). In fact, the orientation of the axial His16 imidazole, with respect to heme, has been shown to be highly conserved in HT and PA (*18*, *19*). Hence, the large difference in the paramagnetic shift pattern of the heme methyl proton signals between the oxidized forms of HT and PA has been interpreted solely in terms of the axial Met61 coordination structure (*26*).

Comparison of the heme methyl proton shifts between the wild-type and mutant proteins for HT and PA showed that the shift patterns of the mutants were almost identical to those of the corresponding wild-type proteins, suggesting that the heme active site structures in the proteins are essentially unaltered by the mutations. Since the shifts of the axial Met61 proton signals resolved in the upfield-shifted region of the spectra of the reduced proteins were almost identical between the mutant and wild-type counterparts (Figure 2B) and, in addition, the differences in the shifts between the corresponding proton signals of the reduced HT(Y27F) and HT were mostly <0.1 ppm (Supporting Information), small shift differences between the mutant and wild-type counterparts may be attributed to the alteration of the chemical environment in the heme active site, due to the removal of the polar OH group of the Tyr27 side chain, located at ∼0.65 nm from heme iron, by the mutations (see below).

Thermostability of the Mutants. We next analyzed the thermostability of the oxidized and reduced forms of the mutants through measurement of CD spectra (200−300 nm) in the temperature range of 30−165 °C at pH 7.0 (*9*). The fractions of the unfolded proteins calculated from the CD ellipticity at 222 nm were plotted against temperature, thermal unfolding profiles for the two mutants in both redox states being obtained (Figure 3). Similar plots for the wild-type proteins are also illustrated, for comparison, in Figure 3. The T_m values of the oxidized and reduced HT(Y27F) were determined to be 116 and 130 °C, respectively, and those of the oxidized and reduced PA(Y27F) to be 91 and 109 °C, respectively (Table 1). Comparison of the T_m value between the mutant and wild-type counterparts showed that the Y27F mutation significantly increases the thermostability of the oxidized proteins, as reflected in the elevation of the T_m value by ∼6 and ∼9 deg for HT and PA, respectively. On the other hand, the T_m values of both the reduced HT and PA were essentially unaltered by the mutations.

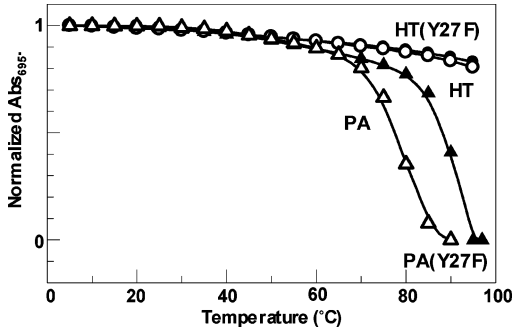

FIGURE 4: Plots of the normalized 695 nm absorption of the oxidized forms of HT (open circles), HT(Y27F) (filled circles), PA (open triangles), and PA(Y27F) (filled triangles) at pH 7.00 against temperature (top). The absorption was normalized in such a way that the values at 5 °C equal 1.0. The dissociation temperatures ($T_{m(Fe-Met)}$) of Fe−Met bonds in the oxidized PA and PA(Y27F) were taken as the midpoints in the plots.

In addition, the stability of the Fe−Met coordination bond in the oxidized forms of the mutants has been analyzed through the temperature dependence of the 695 nm absorption characteristic of the bond (*7*) (Figure 4). The breaking of the Fe−Met bond on thermal denaturation of the protein was clearly manifested in the decrease in absorbance with increasing temperature. In the case of PA(Y27F), the dissociation temperature ($T_{m(Fe-Met)}$) of 89 °C (*12*) was taken as the midpoint in the plots of the normalized absorbance against temperature and is higher by ∼11 deg relative to that of PA (Table 1). Thus, the Fe−Met bond stability in the oxidized PA(Y27F) was significantly enhanced by the mutation. On the other hand, the $T_{m(Fe-Met)}$ values of >100 °C for the oxidized forms of both HT and HT(Y27F), as manifested in the only ∼20% decrease in the absorbance at 95 °C in their plots, hampered quantitative comparison of their Fe−Met bond stability.

The thermostability of the heme active site structure of the oxidized protein can also be analyzed through measurement of ^{1}H NMR spectra at various temperatures (Supporting Information). Although the heme methyl and axial Met61 proton signals of the oxidized PA disappeared completely below 86 °C (*7*), the signals of the oxidized PA(Y27F) could be observed up to 86 °C (Supporting Information), demonstrating the elevated thermostability of the heme active site caused by the mutation. The features of the temperature dependence of the spectra of the oxidized HT(Y27F) were similar to those of the oxidized form of the wild-type counterpart (Supporting Information). The heme methyl and axial Met61 proton signals of the oxidized HT(Y27F) were observed up to 86 °C, reflecting its thermostability, and exhibited anomalous line broadening at low temperatures, due to a dynamic process in the heme active site (*27*−*29*).

pH Profiles of the E_m Values of the Mutants. We next measured the E_m values of the mutants at various pHs, and the obtained values, together with those of the wild-type proteins for comparison, are plotted against pH (E_m−pH plots) in Figure 5. Comparison of the E_m−pH plots between the mutant and wild-type proteins showed that they were quite similar in pattern to each other, the exception being the negative shifts of ∼20 and ∼40 mV for HT(Y27F) and PA(Y27F) relative to those of the wild-type counterparts, respectively, throughout the pH range examined (Figure 5). The pH dependence of the E_m values of the proteins has been

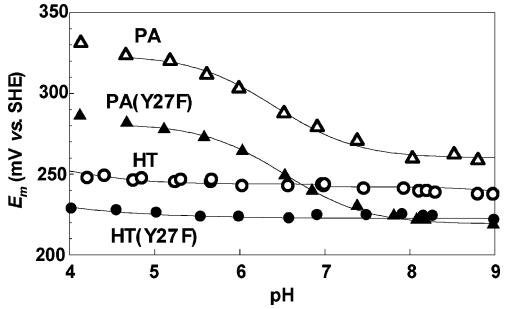

FIGURE 5: (A) Plots of the redox potentials (E_m) against pH for HT (open circles), HY(Y27F) (filled circles), PA (open triangles), and PA(Y27F) (filled triangles) at 25 °C. The E_m−pH plots for the mutant and wild-type proteins were quite similar in pattern to each other, the exception being the negative shifts of ∼20 and ∼40 mV for HT(Y27F) and PA(Y27F) relative to those of the wild-type counterparts, respectively, throughout the pH range.

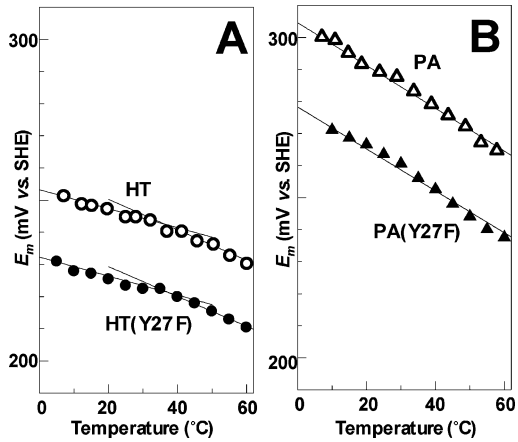

FIGURE 6: Plots of the redox potentials (E_m) against temperature for HT and HT(Y27F) (A) and PA and PA(Y27F) (B) at pH 6.0. The plots for the HT proteins could be fitted by two straight lines with a transition temperature of ∼35 °C, whereas those for the PA proteins exhibited a straight line.

shown to be due to ionization of the heme 17-propionic acid side chain buried in the protein matrix (*10*, *30*−*33*). Consequently, the similarity in the pattern between the E_m−pH plots of the mutant and wild-type proteins indicated that the environment around the heme 17-propionic acid side chain is not affected by the mutation. This result is consistent with the conclusion made on the NMR spectral comparison; i.e., the heme environment is not greatly affected by the mutation. The E_m values of both HT and HT(Y27F) were almost constant throughout the pH range of 4−9, reflecting that the protonation of the heme 17-propionate side chain does not occur in the physiological pH range due to the formation of a hydrogen bond network (see below). Furthermore, the negative shifts of the E_m values of the mutants relative to those of the corresponding wild-type proteins are consistent with our previous finding that a protein with higher stability in its oxidized form exhibits a lower E_m value (*8*, *10*, *12*).

Temperature Dependence of the E_m Values of the Mutants. We also measured the E_m values of the mutants at various temperatures, and the obtained values, together with those of the wild-type proteins for comparison, are plotted against temperature (E_m−T plots) in Figure 6. From the E_m−T plots, we estimated the enthalpic (ΔH) and entropic (ΔS) contributions to the E_m value (Table 1). The plots for the HT proteins could be fitted by two straight lines with a transition

temperature (T_c) of ~35 °C (*12*) (Figure 6). Hence, two sets of values, $\Delta H^{(low)}$ and $\Delta S^{(low)}$ and $\Delta H^{(high)}$ and $\Delta S^{(high)}$, in the temperature ranges of $< T_c$ and $> T_c$, respectively, were determined for these proteins (Table 1). The paramagnetically shifted heme methyl proton signals of the oxidized forms of the proteins at lower temperatures exhibited anomalous line broadening (Supporting Information), which has been proposed to arise from an internal motion of the axial Met61 side chain (*27*−*29*). Hence, the dynamic nature of the Met coordination structure may be responsible for the appearance of the two different protein structures possessing distinctly different thermodynamic parameters. In contrast to the cases of the HT proteins, the E_m-T plots for the PA proteins exhibited a straight line (Figure 6). For both the HT and PA proteins, the obtained ΔS values of the mutants were essentially identical to those of the corresponding wild-type proteins. This finding explicitly indicated that the difference in the E_m value between the mutant and wild-type counterpart is solely enthalpic in origin.

DISCUSSION

Effect of the Mutations on the Heme Environment. The paramagnetically shifted heme methyl and axial Met61 proton signals of the wild-type proteins were slightly affected by the mutations, reflecting a small effect of the mutations on the heme environment. In general, these signals are extremely sensitive to the coordination structures of the axial ligands. But, considering limited freedom for the axial His side chain conformation in cyt *c* as well as the conserved His16 coordination structure in HT and PA (*18*, *19*), it is unlikely that the axial His16 coordination structure is affected by the mutations, although Tyr27 is located near the axial His16 (Figure 1A). Furthermore, since Tyr27 is on the opposite side of axial Met61 relative to the heme plane, with a distance of ~0.94 nm between the Tyr27 OH group and the Met61 sulfur atom (Figure 1A) (*18*), it is also unlikely that the Met61 coordination structure is affected by the mutations. The similarity in the axial Met61 coordination structure between a mutant and the wild-type counterpart was strongly supported by the almost identical ^{1}H NMR shifts for the reduced proteins (Figure 2B, Supporting Information). The paramagnetic shifts of heme methyl proton signals have been shown to be affected by the chemical environment around heme (*34*). Since the removal of the polar OH group of the Tyr27 side chain by the mutations leads to reinforcement of the hydrophobic core near the heme in the protein, the small shift changes in the heme methyl and axial Met61 proton signals of the oxidized proteins, induced by the mutations, could arise from a difference in the heme chemical environment between a mutant and the wild-type counterpart. Thus, the heme active site structures in the proteins are not greatly affected by the mutations, as has been reported for various other mutants.

Effects of the Mutations on Protein Stability. Despite the structural similarity between the mutant and wild-type proteins, the Fe−Met bond stability in the oxidized PA(Y27F) was remarkably greater than that in the oxidized PA (Figure 4), and the oxidized forms of the mutants exhibited remarkably increased thermostability relative to that of the corresponding wild-type counterparts (Figure 3). These results confirmed not only that the Fe−Met bond stability is affected by structural properties of the protein interior (*7*) but also that the increased overall protein stability of the oxidized forms of the mutants is due largely to enhancement of the Fe−Met bond stability through reinforcement of the hydrophobic core of the protein interior by the mutations (*7*, *10*). On the other hand, the thermostability of the reduced proteins remained essentially unaffected by the mutations. These results are consistent with our previous study showing that the stability of an oxidized protein is more greatly affected by a mutation than that of the reduced one (*9*).

Generally, the Fe−Met bond stability in a reduced protein is much greater than that in an oxidized one. The great stability of the Fe−Met bond in a reduced protein has been interpreted in terms of the conventional hard and soft acids and bases principle, which dictates that relatively soft Fe^{2+} forms a more stable bond with the soft thioether sulfur atom of the Met side chain than hard Fe^{3+} does, and the stabilization of the bond due to back-donation of a sulfur atom in the reduced protein (*35*). Hence, owing to the great stability of the Fe−Met bond in the reduced protein, the bond stability in the reduced protein is expected to be considerably less affected by structural properties of the protein interior than that of the oxidized one.

pH Profile of the E_m values of the Mutants. The E_m values of both PA and PA(Y27F) exhibited negative shifts with increasing pH, as shown in Figure 5. The negative shift of the E_m value with increasing pH could be interpreted in terms of the stabilization of cationic ferriheme in the oxidized protein, relative to neutral ferroheme in the reduced one, in the hydrophobic environment of the heme active site through partial neutralization of its positive charge by the heme 17-propionate side chain (*30*, *32*). The similarity in the p*K*a value between PA and PA(Y27F) indicated that the environment of the heme 17-propionate side chain is not affected by the mutation.

The E_m values of both HT and HT(Y27F) were almost constant throughout the physiological pH range, reflecting that the protonation of the heme 17-propionate side chain in the proteins does not occur under these conditions. It has been proposed that the heme propionate side chain buried in the protein matrix of cyt *c* is hydrogen-bonded to the positively charged amino acid side chain of a Lys or Arg residue to lower its pK_a value in order to maintain a constant E_m value throughout the physiological pH range (*31*). The heme 17-propionate side chain buried in the protein interior of HT is not hydrogen-bonded to Lys or Arg but to the side chains of Tyr34, Tyr43, and Trp56 (*18*), and hence its pK_a value appears to be lowered by this unique hydrogen bond network (Supporting Information).

Relationship between Redox Function and Protein Stability. There are two independent mechanisms for the control of the E_m values of hemoproteins. One is a mechanism that regulates the pattern of the pH profile of the E_m value through alteration of the pK_a value of the buried heme 17-propionic acid side chain, as described above, and the other one alters the magnitude of the E_m value throughout a wide pH range. The latter has been shown to occur essentially through the protein's stability (*7*, *8*, *10*).

As reflected in the elevation by ~6 and ~9 deg of the T_m values of the oxidized forms of HT (Y27F) and PA(Y27F) relative to those of the wild-type proteins, respectively (Table 1), the oxidized proteins were greatly stabilized by the mutations. In contrast to the cases of the oxidized proteins,

the stability of the reduced proteins was essentially unaffected by the mutations. Consequently, as expected from the increased stability, HT(Y27F) and PA(Y27F) exhibited negative shifts of ~20 and ~40 mV relative to those of the wild-type counterparts, respectively, this being consistent with our previous finding that a protein with higher stability exhibits a lower E_m value. Consequently, considering a compensatory relationship between high protein stability and a high E_m value (*8*, *10*), the conservation of Tyr27 in the proteins may be responsible for the maintenance of a high E_m value. Or, apart from the control of the E_m value, the presence of Tyr27 in the protein may stem from its ability to form a tyrosyl radical relevant to various biological processes (*36*, *37*).

The thermodynamic analysis of the E_m value demonstrated that the difference in the E_m value between a mutant and the wild-type counterpart is solely enthalpic in origin. Since the stabilities of the mutant and the wild-type counterpart in their reduced forms are almost identical, as reflected in their similar T_m values, the difference in the ΔH value between them is attributed primarily to the difference in the thermodynamic stability of the oxidized protein. Generally, ferriheme in the oxidized protein is less favorable in the hydrophobic protein interior compared with ferroheme in the reduced one. In the mutants, the ferriheme is stabilized to some extent through the stronger Fe−Met bond, leading to regulation of the redox property of the proteins. Thus, the present study provides a typical example of the E_m regulation through the stability of the oxidized protein. Interestingly, the ΔS value was not affected by the mutations (Table 1). This finding indicated not only that the ΔH and ΔS regulations of the E_m value of the protein are independent of each other but also that the ΔS value is not affected by the structural properties of the hydrophobic core in the protein interior. Thus, the present study has successfully provided a molecular basis for quantitative evaluation of the redox function of cyts *c* in terms of their thermodynamic properties. This finding provides novel insights into functional regulation of a protein, which could be utilized for tuning of the E_m value of the protein through protein engineering.

ACKNOWLEDGMENT

We thank Professor Maurizio Brunori (Università di Roma "La Sapienza") for providing the X-ray coordinates of the oxidized HT (PDB code 1YNR (*18*)). We also thank Dr. Jun Hasegawa (Daiichi Pharmaceutical Co., Ltd.) for useful comments. The ^{1}H NMR spectra were recorded on a Bruker AVANCE-600 spectrometer at the Chemical Analysis Center, University of Tsukuba.

SUPPORTING INFORMATION AVAILABLE

A portion of the two-dimensional nuclear Overhauser effect correlated spectrum of the reduced HT(Y27F), a table for ^{1}H NMR shifts of the reduced HT(Y27F) and HT, CD spectra (200−300 nm) of the oxidized and reduced proteins (HT, HT(Y27F), PA, and PA(Y27F)) at pH 7.0 and various temperatures, unfolding profiles of the oxidized and reduced PA(Y27F) at pH 7.0, 600 MHz ^{1}H NMR spectra of the oxidized proteins at pH 7.0 and various temperatures, a schematic representation of the hydrogen bond network of the heme 17-propionate side chain in the oxidized HT, the 695 nm absorption of the oxidized PA and PA(Y27F) at pH 7.0 and various temperatures, and cyclic voltamograms of HT, HT(Y27F), PA, and PA(Y27F) at pH 7.0 and 25 °C. This material is available free of charge via the Internet at http://pubs.acs.org.

REFERENCES

1. Cambillau, C., and Claverie, J. (2000) Structural and genomic correlates of hyperthermostability, *J. Biol. Chem. 275*, 32383−32386.
2. Hasegawa, J., Yoshida, T., Yamazaki, T., Sambongi, Y., Yu, Y., Igarashi, Y., Kodama, T., Yamazaki, K., Kyogoku, Y., and Kobayashi, Y. (1998) Solution structure of thermostable cytochrome *c*-552 from *Hydrogenobacter thermophilus* determined by ^{1}H-NMR spectroscopy, *Biochemistry 37*, 9641−9649.
3. Hasegawa, J., Shimahara, H., Mizutani, M., Uchiyama, S., Arai, H., Ishii, M., Kobayashi, Y., Ferguson, S. J., Sambongi, Y., and Igarashi, Y. (1999) Stabilization of *Pseudomonas aeruginosa* cytochrome c_{551} by systematic amino acid substitutions based on the structure of thermophilic *Hydrogenobacter thermophilus* cytochrome c_{552}, *J. Biol. Chem. 274*, 37533−37537.
4. Hasegawa, J., Uchiyama, S., Tanimoto, Y., Mizutani, M., Kobayashi, Y., Sambongi, Y., and Igarashi, Y. (2000) Selected mutations in a mesophilic cytochrome *c* confer the stability of a thermophilic counterpart, *J. Biol. Chem. 275*, 37824−37828.
5. Uchiyama, S., Hasegawa, J., Tanimoto, Y., Moriguchi, H., Mizutani, M., Igarashi, Y., Sambongi, Y., and Kobayashi, Y. (2002) Thermodynamic characterization of variants of mesophilic cytochrome *c* and its thermophilic counterpart, *Protein Eng. 15*, 455−461.
6. Sambongi, Y., Uchiyama, S., Kobayashi, Y., Igarashi, Y., and Hasegawa, J. (2002) Cytochrome *c* from a thermophilic bacterium has provided insights into the mechanisms of protein maturation, folding, and stability, *Eur. J. Biochem. 269*, 3355−3361.
7. Yamamoto, Y., Terui, N., Tachiiri, N., Minakawa, K., Matsuo, H., Kameda, T., Hasegawa, J., Sambongi, Y., Uchiyama, S., Kobayashi, Y., and Igarashi, Y. (2002) Influence of amino acid side chain packing on Fe-methionine coordination in thermostable cytochrome *c*, *J. Am. Chem. Soc. 124*, 11574−11575.
8. Terui, N., Tachiiri, N., Matsuo, H., Hasegawa, J., Uchiyama, S., Kobayashi, Y., Igarashi, Y., Sambongi, Y., and Yamamoto, Y. (2003) Relationship between redox function and protein stability of cytochromes *c*, *J. Am. Chem. Soc. 125*, 13650−13651.
9. Uchiyama, S., Ohshima, A., Nakamura, S., Hasegawa, J., Terui, N., Takayama, S. J., Yamamoto, Y., Sambongi, Y., and Kobayashi, Y. (2004) Complete thermal-unfolding profiles of oxidized and reduced cytochromes *c*, *J. Am. Chem. Soc. 126*, 14684−14685.
10. Takayama, S. J., Mikami, S., Terui, N., Mita, H., Hasegawa, J., Sambongi, Y., and Yamamoto, Y. (2005) Control of the redox potential of *Pseudomonas aeruginosa* cytochrome c_{551} through the Fe-Met coordination bond strength and pK_a of a buried heme propionic acid side chain, *Biochemistry 44*, 5488−5494.
11. Oikawa, K., Nakamura, S., Sonoyama, T., Ohshima, A., Kobayashi, Y., Takayama, S. J., Yamamoto, Y., Uchiyama, S., Hasegawa, J., and Sambongi, Y. (2005) Five amino acid residues responsible for the high stability of *Hydrogenobacter thermophilus* cytochrome c_{552}, *J. Biol. Chem. 280*, 5527−5532.
12. Takahashi, Y., Takayama, S. J., Mikami, S., Mita, H., Sambongi, Y., and Yamamoto, Y. (2006) Influence of a single amide group on the redox function of *Pseudomonas aeruginosa* cytochrome c_{551}, *Chem. Lett. 35*, 528−529.
13. Sanbongi, Y., Ishii, M., Igarashi, Y., and Kodama, T. (1989) Amino acid sequence of cytochrome c-552 from a thermophilic hydrogen-oxidizing bacterium, *Hydrogenobacter thermophilus*, *J. Bacteriol. 171*, 65−69.
14. Takano, T., and Dickerson, R. E. (1981) Conformation change of cytochrome *c*. I. Ferrocytochrome *c* structure refined at 1.5 Å resolution, *J. Mol. Biol. 153*, 79−94.
15. Takano, T., and Dickerson, R. E. (1981) Conformation change of cytochrome *c*. II. Ferricytochrome *c* refinement at 1.8 Å and comparison with the ferrocytochrome structure, *J. Mol. Biol. 153*, 95−115.
16. Moore, G. R., Pettigrew, G. W., and Rogers, N. K. (1986) Factors influencing redox potentials of electron transfer proteins, *Proc. Natl. Acad. Sci. U.S.A. 83*, 4998−4999.

17. Mauk, A. G., and Moore, R. G. (1997) Control of metalloprotein redox potentials: what does site-directed mutagenesis of hemoproteins tell us?, *J. Biol. Inorg. Chem. 2*, 119−125.
18. Travaglini-Allocatelli, C., Gianni, S., Dubey, V. K., Borgia, A., Di Matteo, A., Bonivento, D., Cutruzzola, F., Bren, K. L., and Brunori, M. (2005) An obligatory intermediate in the folding pathway of cytochrome c_{552} from *Hydrogenobacter thermophilus*, *J. Biol. Chem. 280*, 25729−25734.
19. Matsuura, Y., Takano, T., and Dickerson, R. E. (1982) Structure of cytochrome c_{551} from *Pseudomonas aeruginosa* refined at 1.6 Å resolution and comparison of the two redox forms, *J. Mol. Biol. 156*, 389−409.
20. Taniguchi, I., Iseki, M., Eto, T., Toyosawa, H., Yamaguchi, H., and Yasukouchi, K. (1984) The effect of pH on the temperature dependence of the redox potential of horse heart cytochrome *c* at a bis(4-pyridyl)disulfide-modified gold electrode, *Bioelectrochem. Bioenerg. 13*, 373−383.
21. Ueyama, S., Isoda, S., Hatanaka, H., and Shibano, Y. (1996) Macroscopically rapid electron transfer of cytochrome c_{522} with high thermostability at bare and surface-modified gold electrodes, *J. Electroanal. Chem. 401*, 227−230.
22. Cuttruzzolá, F., Arese, M., Ranghino, G., van Pouderroyen, G., Canters, G., and Brunori, M. (2002) *Pseudomonas aeruginosa* cytochrome C_{551}: probing the role of the hydrophobic patch in electron transfer, *J. Inorg. Biochem. 88*, 353−361.
23. La Mar, G. N., Satterlee, J. D., and de Ropp, J. S. (2000) Nuclear magnetic resonance of hemoproteins, in *The Porphyrin Handbook* (Kadish, K., Smith, K. M., and Guilard, R., Eds.) pp 185−298, Academic Press, New York.
24. Bertini, I., and Luchinat, C. (1986) *NMR of Paramagnetic Molecules in Biological Systems*, pp 19−46, The Benjamin/Cummings Publishing Co., Menlo Park, CA.
25. Yamamoto, Y. (1998) NMR study of active sites in paramagnetic hemoproteins, *Annu. Rep. NMR Spectrosc. 36*, 1−77.
26. Tachiiri, N., Hemmi, H., Takayama, S. J., Mita, H., Hasegawa, J., Sambongi, Y., and Yamamoto, Y. (2004) Effects of axial methionine coordination on the in-plane asymmetry of the heme electronic structure of cytochrome *c*, *J. Biol. Inorg. Chem. 9*, 733−742.
27. Zhong, L., Wen, X., Rabinowitz, T. M., Russell, B. S., Karan, E. F., and Bren, K. L. (2004) Heme axial methionine fluxionality in *Hydrogenobacter thermophilus* cytochrome c_{552}, *Proc. Natl. Acad. Sci. U.S.A. 101*, 8637−8642.
28. Wen, X., and Bren, K. L. (2005) Suppression of axial methionine fluxion in *Hydrogenobacter thermophilus* Gln64Asn cytochrome c_{552}, *Biochemistry 44*, 5225−5233.
29. Wen, X., and Bren, K. L. (2005) Heme axial methionine fluxion in *Pseudomonas aeruginosa* Asn64Gln cytochrome c_{551}, *Inorg. Chem. 44*, 8587−8593.
30. Leitch, F. A., Moore, G. R., and Pettigrew, G. W. (1984) Structural basis for the variation of pH-dependent redox potentials of *Pseudomonas* cytochromes *c-551*, *Biochemistry 23*, 1831−1838.
31. Moore, G. R., Pettigrew, G. W., Pitt, R. C., and Williams, R. J. P. (1980) pH dependence of the redox potential of *Pseudomonas aeruginosa* cytochrome *c*-551, *Biochim. Biophys. Acta 590*, 261−271.
32. Moore, G. R. (1983) Control of redox properties of cytochrome *c* by special electrostatic interactions, *FEBS Lett. 161*, 171−175.
33. Cutler, R. L., Davies, A. M., Creighton, S., Warshel, A., Moore, G. R., Smith, M., and Mauk, A. G. (1989) Role of arginine-38 in regulation of the cytochrome *c* oxidation-reduction equilibrium, *Biochemistry 28*, 3188−3197.
34. Misumi, Y., Terui, N., and Yamamoto, Y. (2002) Structural characterization of non-native states of sperm whale myoglobin in aqueous ethanol of 2,2,2-trifluoroethanol media, *Biochim. Biophys. Acta 1601*, 75−84.
35. Rovira, C., Carloni, P., and Parrinello, M. (1999) The iron-sulfur bond in cytochrome *c*, *J. Phys. Chem. B 103*, 7031−7035.
36. Stubbe, J., and van der Donk, W. A. (1998) Protein radicals in enzyme catalysis, *Chem. Rev. 98*, 705−762.
37. Stubbe, J. (2003) Radicals with a controlled lifestyle, *Chem. Commun.*, 2511−2513.
38. Murshudov, G. N., Vagin, A. A., Lebedev, A., Wilson, K. S., and Dodcon, E. J. (1999) Efficient anisotropic refinement of macromolecular structures using FFT, *Acta Crystallogr. D55*, 247−255.
39. DeLano, W. L. (2002) The PyMOL molecular graphics system on http://www.pymol.org.

BI061164G